In silico integration of thousands of epigenetic datasets into 707 cell type regulatory annotations improves the trans-ethnic portability of polygenic risk scores

Tiffany Amariuta*[1-5], Kazuyoshi Ishigaki*[1-3,6], Hiroki Sugishita[7], Tazro Ohta[8,9], Koichi Matsuda[10,11], Yoshinori Murakami[12], Alkes L. Price[3,13,14], Eiryo Kawakami[8,15], Chikashi Terao[6,16,17], Soumya Raychaudhuri[1-5,18]

[1]Center for Data Sciences, Harvard Medical School, Boston, Massachusetts, 02115, USA.
[2]Divisions of Genetics and Rheumatology, Department of Medicine, Brigham and Women's Hospital, Harvard Medical School, Boston, Massachusetts, 02115, USA.
[3]Program in Medical and Population Genetics, Broad Institute of MIT and Harvard, Cambridge, Massachusetts, 02142, USA.
[4]Department of Biomedical Informatics, Harvard Medical School, Boston, Massachusetts, 02115, USA.
[5]Graduate School of Arts and Sciences, Harvard University, Cambridge, Massachusetts, 02138, USA.
[6]Laboratory for Statistical and Translational Genetics, RIKEN Center for Integrative Medical Sciences, Kanagawa, 230-0045 Japan.
[7]Laboratory for Developmental Genetics, RIKEN Center for Integrative Medical Sciences (IMS), Kanagawa, Japan
[8]Medical Sciences Innovation Hub Program, RIKEN, Kanagawa, Japan.
[9]Database Center for Life Science, Joint Support-Center for Data Science Research, Research Organization of Information and Systems, Shizuoka, Japan.
[10]Laboratory of Genome Technology, Human Genome Center, Institute of Medical Science, The University of Tokyo, Tokyo, 108-8639 Japan.
[11]Laboratory of Clinical Genome Sequencing, Department of Computational Biology and Medical Sciences, Graduate School of Frontier Sciences, The University of Tokyo, Tokyo, 108-8639 Japan.
[12]Division of Molecular Pathology, Institute of Medical Science, The University of Tokyo, Tokyo, 108-8639 Japan
[13]Department of Epidemiology, Harvard T.H. Chan School of Public Health, Boston, MA 02115, USA.
[14]Department of Biostatistics, Harvard T.H. Chan School of Public Health, Boston, MA 02115, USA.
[15]Artificial Intelligence Medicine, Graduate School of Medicine, Chiba University, Chiba, Japan.
[16]Clinical Research Center, Shizuoka General Hospital, Shizuoka, 420-8527 Japan.
[17]The Department of Applied Genetics, The School of Pharmaceutical Sciences, University of Shizuoka, Shizuoka, 422-8526 Japan.
[18]Centre for Genetics and Genomics Versus Arthritis, Centre for Musculoskeletal Research, Manchester Academic Health Science Centre, The University of Manchester, Manchester, UK.

*indicates equal contributions
**Correspondence to Soumya Raychaudhuri, soumya@broadinstitute.org

Abstract

Poor trans-ethnic portability of polygenic risk score (PRS) models is a critical issue that may be partially due to limited knowledge of causal variants shared among populations. Hence, leveraging noncoding regulatory annotations that capture genetic variation across populations has the potential to enhance the trans-ethnic portability of PRS. To this end, we constructed a unique resource of 707 cell-type-specific IMPACT regulatory annotations by aggregating 5,345 public epigenetic datasets to predict binding patterns of 142 cell-type-regulating transcription factors across 245 cell types. With this resource, we partitioned the common SNP heritability of diverse polygenic traits and diseases from 111 GWAS summary statistics of European (EUR, average N=180K) and East Asian (EAS, average N=157K) origin. For 95 traits, we were able to identify a single IMPACT annotation most strongly enriched for trait heritability. Across traits, these annotations captured an average of 43.3% of heritability (se = 13.8%) with the top 5% of SNPs. Strikingly, we observed highly concordant polygenic trait regulation between populations: the same regulatory annotations captured statistically indistinguishable SNP heritability (fitted slope = 0.98, se = 0.04). Since IMPACT annotations capture both large and consistent proportions of heritability across populations, prioritizing variants in IMPACT regulatory elements may improve the trans-ethnic portability of PRS. Indeed, we observed that EUR PRS models more accurately predicted 21 tested phenotypes of EAS individuals when variants were prioritized by key IMPACT tracks (49.9% mean relative increase in R^2). Notably, the improvement afforded by IMPACT was greater in the trans-ethnic EUR-to-EAS PRS application than in the EAS-to-EAS application (47.3% vs 20.9%, P < 1.7e-4). Overall, our study identifies a crucial role for functional annotations such as IMPACT to improve the trans-ethnic portability of

genetic data, and this has important implications for future risk prediction models that work across populations.

Introduction

An important challenge for complex trait genetics is that there is no clear framework to transfer population-specific genetic data, such as GWAS results, to individuals of other ancestries[1–3]. The importance of this challenge is accentuated by the fact that 80% of all genetic studies have been performed using individuals of European ancestry, accounting for a minority of the world's population[4]. This is exacerbated by the fact that population-specific linkage disequilibrium (LD) between variants confounds inferences about causal cell types and variants (**Figure 1A**)[5–7]. GWAS have the potential to revolutionize the clinical application and utility of genetic data to the individual, exemplified by current polygenic risk score (PRS) models[5,8–16]. However, while the utility of PRS models relies on accurate estimation of allelic effect sizes from GWAS and benefits from genetic similarity between the test cohort and the GWAS cohort, recent studies have explicitly observed a lack of trans-ethnic portability[2,3,5,8,17,18]. Previous studies have extensively shown that functional annotations can improve PRS models when learned and applied to the same population[19,20], by introducing biologically-relevant priors on causal effect sizes and compensating for inflation of association statistics by LD. However, the potential for functional annotations to improve trans-ethnic PRS frameworks, where the influences of population-specific LD are more profound, has not yet been extensively investigated.

However, designing functional annotations that may improve PRS models is challenging. While the genetic variation of a complex trait likely regulates diverse biological mechanisms genome-wide, such functional annotations must strike a balance of specificity, comprehensively but precisely capturing large regulatory programs. Pinpointing these mechanisms is especially difficult as genome-wide association studies (GWAS) have identified thousands of genetic associations with complex phenotypes[8,21–23]. It has been estimated that about 90% of these associations reside in protein noncoding regions of the genome, making their mechanisms difficult to interpret[24,25]. Defining the etiology of complex traits and diseases requires knowledge of phenotyping-driving cell types in which these associated variants act. Transcription factors (TFs) are poised to orchestrate large polygenic regulatory programs as genetic variation in their target regions can modulate gene expression, often in cell-type-specific contexts[26,27]. Genomic annotations marking the precise location of TF-mediated cell type regulation can be exploited to elucidate the genetic basis of polygenic traits. However, currently there is no comprehensive catalogue of the binding profiles of the approximately 1,600 human TFs in every known cell type[28]. Moreover, existing TF ChIP-seq datasets are limited to factors with effective antibodies and suffer from inter-experimental variation, noise, and genomic bias[29,30].

To overcome these challenges, we previously developed IMPACT, a genome-wide cell-type-specific regulatory annotation strategy that models the epigenetic pattern around active TF binding using linear combinations of functional annotations[31]. In rheumatoid arthritis (RA), IMPACT CD4+ T cell annotations captured substantially more heritability than functional annotations derived from single experiments, including TF and histone modification ChIP-seq[6]. In this study, we expanded this approach by aggregating 5,345 functional annotations with

116 IMPACT to create a powerful and generalizable resource of 707 cell-type-specific gene
117 regulatory annotations (**Web Resources**) based on binding profiles of 142 TFs across 245 cell
118 types (**Figure 1B,C**). This study builds on our previous study introducing IMPACT, in which we
119 created only 13 annotations (13 TFs) based on 515 functional annotations. Assuming that causal
120 variants are largely shared between populations[2,21], we hypothesized that restricting PRS
121 models to variants within trait-relevant IMPACT annotations, which are more likely to have
122 regulatory roles and less likely to be confounded by LD, will especially improve their trans-
123 ethnic portability.

124 In this study, we identify key IMPACT regulatory annotations that capture genome-wide
125 polygenic mechanisms underlying a diverse set of complex traits, supported by enrichments of
126 genetic heritability, multi-ethnic marginal effect size correlation (a mechanism of improved
127 PRS), and improved trans-ethnic portability of PRS models (**Figure 1D**). Here, we defined and
128 employed our compendium of 707 IMPACT regulatory annotations to study polygenic traits and
129 diseases from 111 GWAS summary datasets of European (EUR) and East Asian (EAS) origin.
130 Assuming shared causal variants between populations, annotations that prioritize shared
131 regulatory variants must (1) capture disproportionately large amounts of genetic heritability in
132 both populations, (2) be enriched for multi-ethnic marginal effect size correlation, and (3)
133 improve the trans-ethnic applicability of population-specific PRS models. Using our
134 compendium of regulatory annotations, we identified key annotations for each polygenic trait
135 and demonstrated their utility in each of these three applications toward prioritization of
136 shared regulatory variants. Overall, this work improves the interpretation and trans-ethnic
137 portability of genetic data and provides implications for future clinical implementations of risk
138 prediction models.

Figure 1

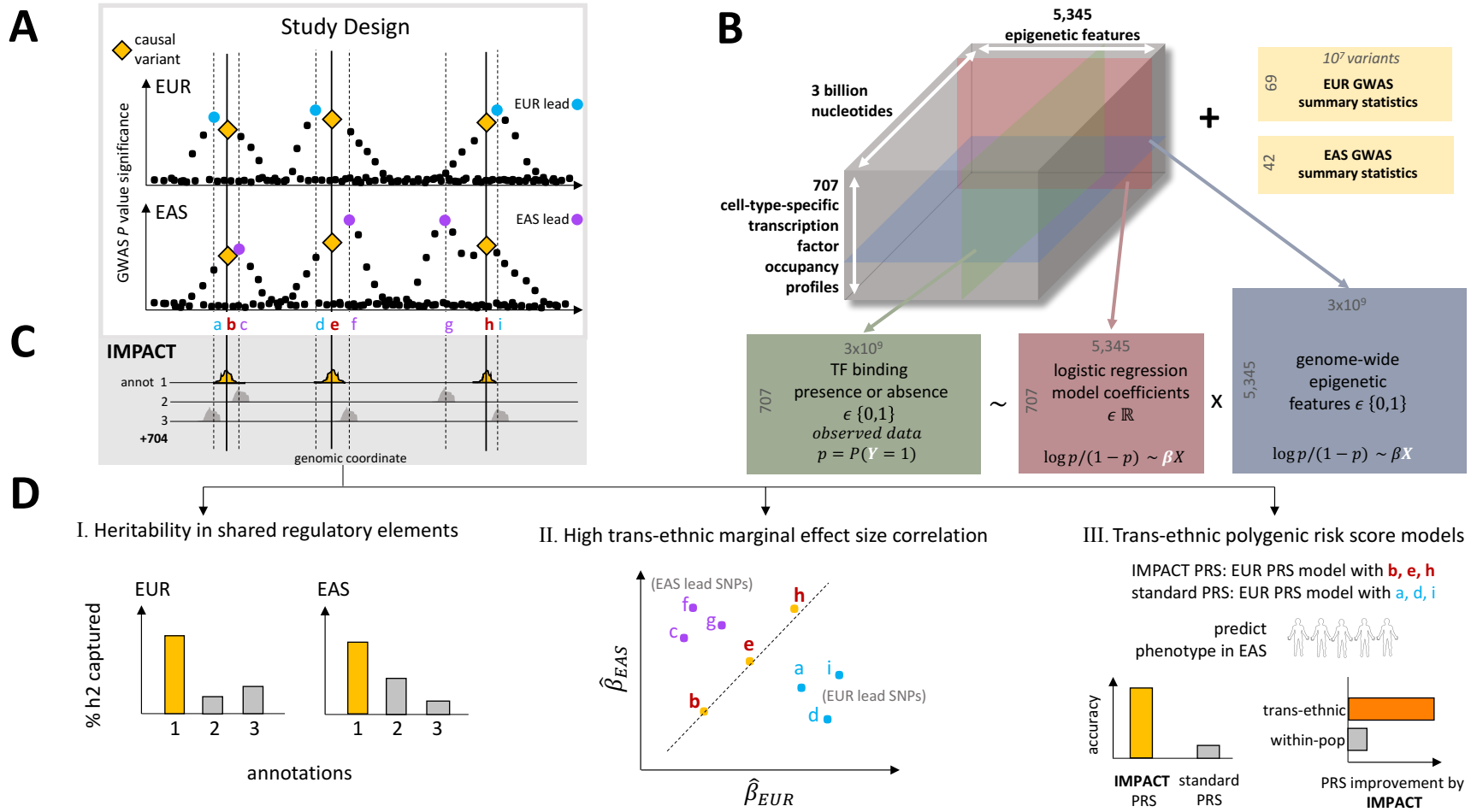

Figure 1 legend. Study design to identify regulatory annotations that prioritize regulatory variants in a multi-ethnic setting. A) Population-specific LD confounding and subsequent inflation of GWAS associations complicate the interpretation of summary statistics and transferability to other populations; functional data may help improve trans-ethnic genetic portability. B) Prism of functional data in IMPACT model: 707 genome-wide TF occupancy profiles (green), 5,345 genome-wide epigenomic feature profiles (blue), and fitted weights for these features (pink) to predict TF binding by logistic regression. Using IMPACT annotations, we investigate 111 GWAS summary datasets (yellow) of EUR and EAS origin. C) Compendium of 707 genome-wide cell-type-specific IMPACT regulatory annotations. D) Annotations that prioritize common regulatory variants must I) capture large proportions of heritability in both populations, II) account for consistent effect size estimations between populations and III) improve the trans-ethnic application of PRS.

139

140 ## Results

141

142 **Building a compendium of *in silico* gene regulatory annotations**

143

144 To capture genetic heritability of diverse polygenic diseases and quantitative traits, we
145 constructed a comprehensive compendium of 707 cell type regulatory annotation tracks. To do
146 this, we applied the IMPACT[31] framework to 707 unique TF-cell type pairs obtained from a total
147 of 3,181 TF ChIP-seq datasets from NCBI, representing 245 cell types and 142 TFs (**Figure 1B**,
148 **Online Methods**, **Web Resources**, **ST1**, **SF1**)[32]. Briefly, IMPACT learns an epigenetic signature of
149 active TF binding evidenced by ChIP-seq, differentiating bound from unbound TF sequence
150 motifs using logistic regression. We derive this signature from 5,345 epigenetic and sequence
151 features, predominantly generated by ENCODE[33] and Roadmap[34] (**Online Methods**, **ST2**); these
152 data were drawn from diverse cell types, representing the biological range of the 707 candidate
153 models. IMPACT then probabilistically annotates the genome, e.g. on a scale from 0 to 1,
154 without using the TF motif, identifying regulatory regions that are similar to those that the TF
155 binds.

156 To assess the specificity of our IMPACT annotations, we test whether they (1) accurately
157 predict binding of the modeled TF, (2) share cell-type-specific characteristics with other tracks
158 of the same cell type, and (3) score cell-type-specifically expressed genes higher than
159 nonspecific genes. The 707 models that we defined had a high TF binding prediction accuracy
160 with mean AUPRC = 0.74 (se = 0.008, **SF2**) using cross-validation. Annotations segregated by cell
161 type rather than by TF, excluding CTCF, suggesting a single TF may bind to different enhancers

162 in different cell types (**Figure 2A**). Annotations of the same cell types were more strongly
163 correlated genome-wide (Pearson r = 0.56, se = 0.06) than annotations of different cell types
164 (Pearson r = 0.48, se = 0.003, difference of means P < 0.03, **SF2**). Furthermore, the covariance
165 structure between TF ChIP-seq training datasets is similar to that of corresponding IMPACT
166 annotations, indicating that the IMPACT model does not introduce spurious correlations among
167 unrelated ChIP-seq datasets (**SF2**). Lastly, for nine different cell types, we examined cell-type-
168 specifically expressed genes from Finucane et al[35] and corresponding differential expression t-
169 statistics. We observed significantly larger IMPACT probabilities at SNPs in and near these genes
170 (mean = 0.062, se = 0.011) compared to genes that were generally expressed (mean = 0.045, se
171 = 0.006; difference of means P = 0.024, **Figure 2B**, **SF2**, **Online Methods**), suggesting that
172 IMPACT annotates relevant cell type regulatory elements.
173
174 **Partitioning common SNP heritability of 111 GWAS summary statistics in EUR and EAS**
175
176 We obtained summary statistics from 111 publicly available GWAS summary statistics
177 for diverse polygenic traits and diseases. Throughout the text, we use five randomly selected
178 traits to exemplify our results: asthma, RA, prostate cancer (PrCa), mean corpuscular volume
179 (MCV), and body height. These included 69 from EUR participants[31,36] (average N = 180K,
180 average heritability z-score = 12.9, 41/69 from UK BioBank)[6,37] and 42 from EAS participants of
181 BioBank Japan[3,38–40] (average N = 157K, average heritability z-score = 6.6)[22] (**ST3**). All of the
182 summary statistics used were generated from studies that had a sample size greater than
183 10,000 individuals and also had a significantly non-zero heritability (z-score > 1.97). There are
184 29 phenotypes for which we obtained summary statistics in both EUR and EAS. Although 10/29

Figure 2

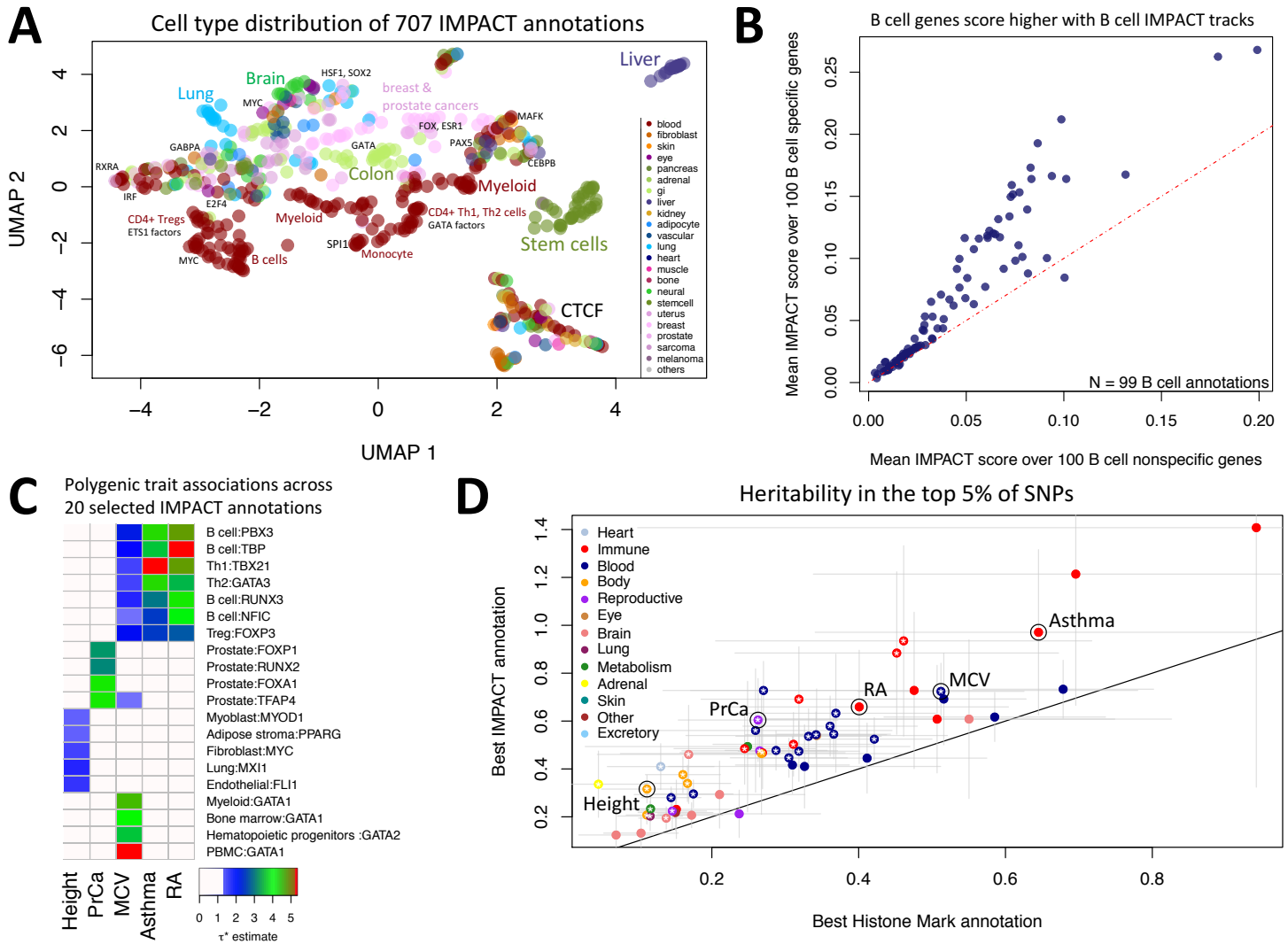

Figure 2 legend. IMPACT annotates relevant cell type regulatory elements. A) Low-dimensional embedding and clustering of 707 IMPACT annotations using uniform manifold approximation projection (UMAP). Annotations colored by cell type category; TF groups indicated where applicable. B) IMPACT annotates cell type specifically expressed genes with higher scores than nonspecific genes. C) Biologically distinct regulatory modules revealed by cell type-trait associations with significantly nonzero τ^* across 20 of 707 IMPACT regulatory annotations and 5 representative EUR complex traits, color indicates -$\log_{10}$ FDR 5% adjusted P value of τ^*. D) Lead IMPACT annotations capture more heritability than lead cell-type-specific histone modifications across 60 of 69 EUR summary statistics for which a lead IMPACT annotation was identified. * indicates heritability estimate difference of means $P < 0.05$.

185 traits have a multi-ethnic genetic correlation (R_g) significantly less than 1 (P < 0.05/29 tested
186 traits), overall we observed high R_g for most traits, supporting our assumption that causal
187 variants are generally shared across populations (**Online Methods**, **SF3**)[41]. At two extremes,
188 basophil count has a low multi-ethnic R_g of 0.32 (sd = 0.10), while atrial fibrillation has a high
189 multi-ethnic R_g of 0.98 (sd = 0.11), consistent with previous observations made using *Popcorn*,
190 but using different parameter estimation strategies (**Online Methods**)[3].

191 We then partitioned the common SNP (minor allele frequency (MAF) > 5%) heritability
192 of these 111 datasets using S-LDSC[6] with an adapted baseline-LD model excluding cell-type-
193 specific annotations[31,36] (**SF3, Online Methods**). Next, we tested each of the traits against each
194 of the 707 IMPACT annotations, assessing the significance of a non-zero τ^*, which is defined as
195 the proportionate change in per-SNP heritability associated with a one standard deviation
196 increase in the value of the annotation (**Online Methods**)[36]. We observed that 95 phenotypes
197 had at least one significant annotation-trait association (τ^* > 0, two-tailed FDR < 5%, **Ext. Data**
198 **1, Online Methods**, **ST4-8**). Here, we highlight associations with EUR summary statistics for the
199 five exemplary phenotypes mentioned above: asthma, RA, PrCa, MCV, and height (**Figure 2C**).
200 Consistent with known biology, B and T cells were strongly associated with asthma[42], RA[43], and
201 MCV[44,45] while other blood cell regulatory annotations predominantly derived from GATA
202 factors were also associated with MCV. Prostate cancer cell lines were associated with PrCa,
203 while many cell types including myoblasts[46], fibroblasts[47], and adipocytes[48,49], lung cells, and
204 endothelial cells were associated with height, perhaps related to musculo-skeletal
205 developmental pathways.

206 For each trait, we defined the lead IMPACT regulatory annotation as the annotation
207 capturing the greatest per-SNP heritability, e.g. the largest while significant τ^* estimate (**ST9**).

208 With their top 5% of SNPs, lead IMPACT annotations captured an average of 43.3% heritability
209 (se = 13.8%) across these 95 polygenic traits (**SF4**, **Online Methods**), with more than 25% of
210 heritability captured for two-thirds of the tested summary statistics (73/111 traits) and more
211 than 50% captured for 28% (31/111). Returning to our five exemplary phenotypes, with the top
212 5% of EUR SNPs, IMPACT captured 97.1% (sd = 17.6%) of asthma heritability with the T-bet Th1
213 annotation, 65.9% (sd = 12.1%) of RA heritability with the B cell TBP annotation, 60.4% (sd =
214 8.9%) of PrCa heritability with the prostate cancer cell line (LNCAP) TFAP4 annotation, 72.4%
215 (sd = 6.0%) of MCV heritability with the GATA1 PBMC annotation, and lastly 31.6% (sd = 3.0%)
216 of height heritability with the lung MXI1 annotation (**Figure 2D**). While the observed association
217 between lung and height is not intuitive, within the MXI1 gene lies a genome-wide significant
218 variant associated with height[50]. Moreover, we captured significantly more heritability across
219 EUR traits using our expanded set of 707 IMPACT annotations (mean = 49.5%, se = 12.0%)
220 compared to the 13 annotations in our previous study (mean = 32.3%, se = 1.3%, difference of
221 means P = 0.02).
222 To demonstrate the value of IMPACT tracks, we compared them to annotations derived
223 from single experimental assays. For example, since each of the IMPACT tracks was trained on
224 TF ChIP-seq data, we directly compared the heritability captured by both data types. We
225 observed that the heritability captured by lead IMPACT annotations (mean τ^* = 3.53, se = 0.91)
226 was significantly greater than by the analogous TF ChIP-seq used in training (mean τ^* = 1.71, se
227 = 0.94, difference of means P = 0.02). We also compared IMPACT tracks to histone marks, which
228 are commonly used to quantify cell type heritability[6]. From 220 publicly available cell-type-
229 specific histone mark ChIP-seq annotations of EUR SNPs[6], we selected the lead histone mark
230 track for each of 69 EUR summary statistics. Restricting to the top 5% of SNPs, we observed that

231 the mean EUR heritability captured by lead IMPACT annotations (49.5%, se = 12.0%) was
232 significantly greater than by lead histone mark annotations (28.4%, se = 9.0%, difference of
233 means *P* = 0.02) (**Figure 2D, ST10**). For example, the lead IMPACT annotation for asthma
234 captured 1.5x more heritability than the best histone mark annotation (H3K27ac in CD4+ Th2),
235 capturing 64.2% (sd = 15.5%) of heritability. Similarly, IMPACT captured 1.7x more RA
236 heritability than H3K4me3 in CD4+ Th17s; IMPACT captured 1.4x more MCV heritability than
237 H3K4me3 in CD34+ cells; IMPACT captured 2.3x more PrCa heritability than H3K4me3 in CD34+
238 cells; and IMPACT captured 3.1x more height heritability than H3K4me3 in lung cells. In terms
239 of τ^*, IMPACT also captured more per-SNP heritability than histone marks: mean τ^* fold
240 change = 1.38x (**SF5**).

241 Since some of our IMPACT annotations are similar to each other (**SF2**), we performed
242 serial conditional analyses in order to identify IMPACT annotations explaining heritability
243 independently from one another (**Online Methods**). This strategy might identify complex traits
244 for which several distinct biological mechanisms are independently regulated by genetic
245 variation. Indeed, we identified 30 EUR phenotypes and 8 EAS phenotypes with multiple
246 independent IMPACT associations (**SF6**, **ST11-12**). For example, four annotations were
247 independently associated with EUR PrCa: prostate (TFAP4), prostate (RUNX2), mesendoderm
248 (PDX1), and cervix (NFYB). Moreover, for seven EUR traits, three IMPACT annotations were
249 independently associated: height (adipocytes, fibroblasts, lung), neutrophil count (monocytes,
250 adipocytes, B cells), osteoporosis (myoblasts, mesenchymal stem cells, cervix), IBD (T cells and
251 two B cell annotations), platelet count (PBMCs, hematopoietic progenitors, muscle), systolic
252 blood pressure (endothelial, mesenchymal stem cells, fibroblasts), and white blood cell count (B
253 cells, adipocytes, hematopoietic progenitors). We found that the heritability z-score, an index

254 correlated with the power of S-LDSC[6], is strongly predictive of the number of independent
255 regulatory associations (linear regression $P < 5.4e-9$), while sample size is not (linear regression
256 $P = 0.19$) (**SF7**). Our findings suggest that multiple independent regulatory programs can
257 contribute to the heritability of complex traits, and we can detect them when phenotypes are
258 sufficiently heritable and the GWAS provide accurate effect size estimation.
259
260 **Concordance of polygenic regulation between European and East Asian populations**
261
262 Previous studies have shown concordance of polygenic effects between EUR and EAS
263 individuals in RA[1] and between EUR and African American individuals in PrCa[51]. However, to our
264 knowledge, the extent of these shared effects has not yet been comprehensively investigated
265 across many functional annotations and in diverse traits. Here, we quantified the SNP
266 heritability (τ^*) of 29 traits in EUR and EAS captured by a set of approximately 100 independent
267 IMPACT regulatory annotations (**Figure 3B, SF8, Online Methods**). Assuming shared causal
268 variants in EUR and EAS, IMPACT annotations that best prioritize shared genomic regions
269 regulating a phenotype presumably also disproportionately capture similar amounts of
270 heritability in both EUR and EAS (**Figure 1D-I**, **Figure 3A**). Briefly, we selected independent
271 annotations using an iterative pruning approach: for each trait, we ranked all annotations by τ^*
272 and removed any annotation correlated with Pearson $r > 0.5$ to the lead annotation and then
273 repeated. As IMPACT annotations are independent of population-specific factors including LD
274 and allele frequencies (**SF3**), they are poised to capture the genome-wide distribution of
275 regulatory variation in a population-independent manner. We observed that τ^* estimates
276 across annotations for EUR and EAS are strikingly similar, with a regression coefficient that is

Figure 3

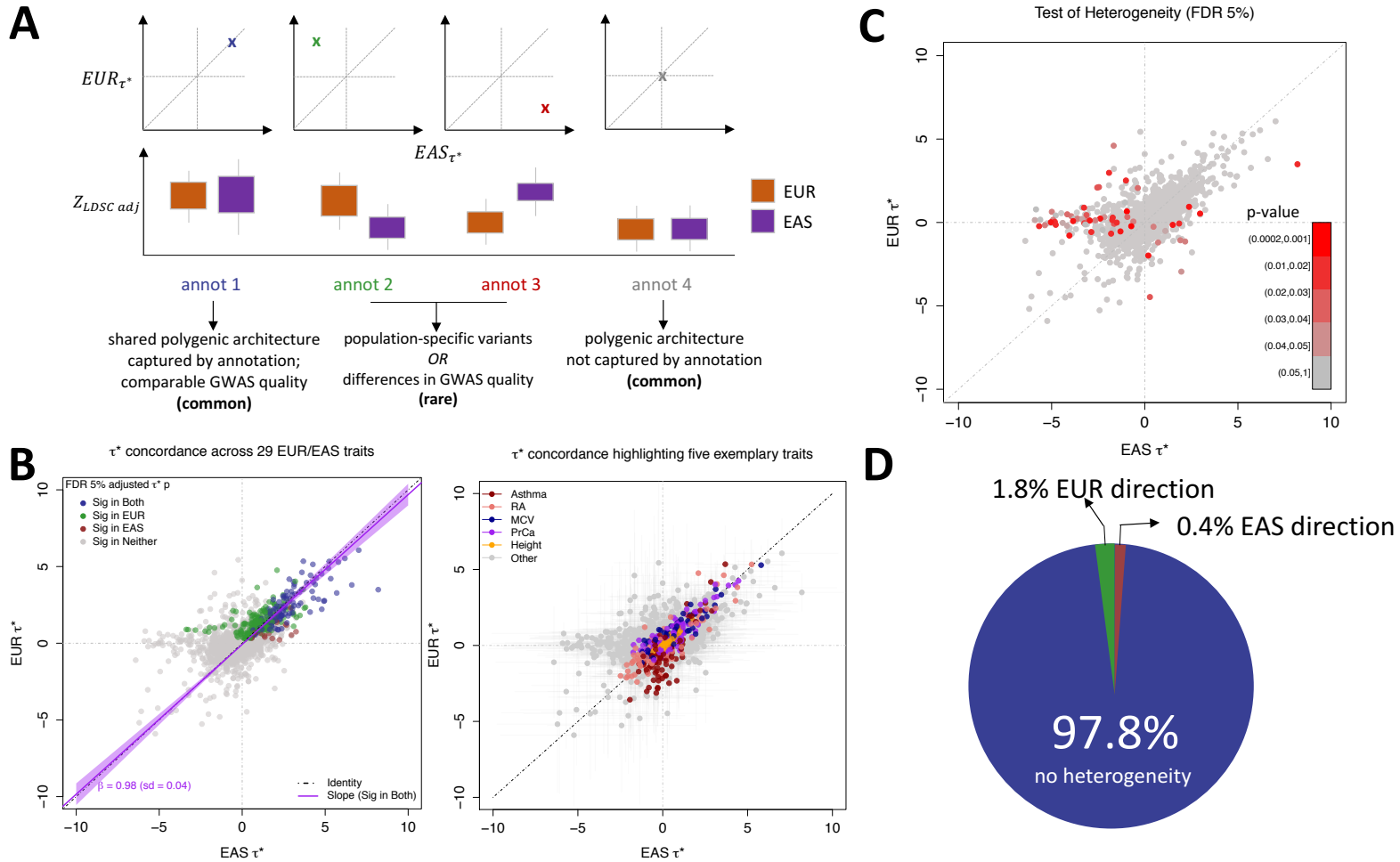

Figure 3 legend. Multi-ethnic concordance of regulatory elements defined by IMPACT. A) Illustrative concept of concordance versus discordance of τ^* between populations. Concordance implies a similar distribution of causal variants and effects captured by the same annotation. The implications of discordant τ^* are not as straightforward. B) Common per-SNP heritability (τ^*) estimate for sets of independent IMPACT annotations across 29 traits shared between EUR and EAS. Left: color indicates τ^* significance (τ^* greater than 0 at 5% FDR) in both populations (blue), significant in only EUR (green), significant in only EAS (red), significant in neither (gray). Line of best fit through annotations significant in both populations (dark purple line, 95% CI in light purple). Black dotted line is the identity line, y = x. Right: color indicates association to one of five exemplary traits. C) Heterogeneity test at 5% FDR for annotation-trait associations between EUR and EAS. Color indicates significance of difference of means *P* value. D) Heterogeneity test reveals 2.2% of all annotation-trait associations with significantly discordant τ^* estimates between populations.

277 consistent with identity (slope = 0.98, se = 0.04). For example, we observed a strong Pearson
278 correlation of τ^* between EUR and EAS for asthma (r = 0.98), RA (r = 0.87), MCV (r = 0.96), PrCa
279 (r = 0.90), and height (r = 0.96). Furthermore, we found that 97.8% of our τ^* estimates have no
280 evidence of population heterogeneity (FDR P > 0.05) (**Figure 3C**). Among our five representative
281 traits, we observed only one instance of heterogeneity, in which the B cell SRF IMPACT
282 annotation captured RA heritability significantly more in EUR than in EAS (EUR τ^* = 1.20 (se =
283 0.40), EAS τ^* = -1.06 (se = 0.46), difference of means P < 2.0e-4). Overall, our results suggest
284 that regulatory variants in EUR and EAS populations are equally enriched within the same
285 classes of regulatory elements. This does not exclude the possibility of population-specific
286 variants or causal effect sizes, as evidenced by 10 traits with multi-ethnic genetic correlation
287 significantly less than 1. Rather, these results suggest that causal biology, including disease-
288 driving cell types and their regulatory elements, underlying polygenic traits and diseases, is
289 largely shared between these populations.
290
291 **Models incorporating IMPACT functional annotations improve the trans-ethnic portability of**
292 **polygenic risk scores**
293
294 PRS models have great clinical potential: previous studies have shown that individuals
295 with higher PRS have increased risk for disease[8–12]. In the future, polygenic risk assessment may
296 become as common as screening for known mutations of monogenic disease, especially as it
297 has been shown that individuals with severely high PRS may be at similar risk to disease as are
298 carriers of rare monogenic mutations[12]. However, since PRS heavily rely on GWAS with large
299 sample sizes to accurately estimate effect sizes, there is specific demand for the transferability

300 of PRS from populations with larger GWAS to populations underrepresented by
301 GWAS[2,3,5,8,17,18,20]. As we would like to investigate the ability of IMPACT annotations to improve
302 the trans-ethnic application of PRS, we chose pruning and thresholding (P+T) as our model[3,8].
303 We elected to use P+T rather than LDpred[5,20] or AnnoPred[19], which compute a posterior effect
304 size estimate for all SNPs genome-wide based on membership to functional categories. With
305 P+T, we can partition the genome by IMPACT-prioritized and deprioritized SNPs, whereas the
306 assumptions of the LDpred and AnnoPred models do not support the removal of variants,
307 making it difficult to directly assess improvement due to IMPACT prioritization. Moreover,
308 these models have not been explicitly designed or tested for the trans-ethnic application of PRS
309 and thus are beyond the scope of our work. We conventionally define PRS as the product of
310 marginal SNP effect size estimates and imputed allelic dosage (ranging from 0 to 2), summed
311 over M SNPs in the model. Conventional P+T utilizes marginal effect size estimates and
312 therefore is susceptible to selecting a tagging variant over the causal one guided by GWAS *P*
313 values that are inflated by LD. Therefore, we hypothesized that any observed improvement due
314 to incorporation of IMPACT annotations could result from prioritization of variants with higher
315 marginal multi-ethnic effect size correlation (**Figure 1D-II**).
316 Hence, we tested this hypothesis before assessing PRS performance. We selected 21 of
317 29 summary statistics shared between EUR and EAS with an identified lead IMPACT association
318 in both populations. Then, using EUR lead IMPACT annotations for each trait (**ST9**), we
319 partitioned the genome three ways: (1) the SNPs within the top 5% of the IMPACT annotation,
320 (2) the SNPs within the bottom 95% of the IMPACT annotation, and (3) the set of all SNPs
321 genome-wide (with no IMPACT prioritization). We then performed stringent LD pruning ($r^2 < 0.1$
322 from EUR individuals of phase 3 of 1000 Genomes[52]), guided by the EUR GWAS *P* value, to

323 acquire sets of independent SNPs in order to compute a EUR-EAS marginal effect size estimate
324 correlation (**Online Methods**).
325 For example, in height, EUR-EAS effect size estimates of SNPs in the top 5% partition
326 (Pearson r = 0.434, **Figure 4A**) are 11.4-fold more similar than those in the bottom 95%
327 partition (r = 0.038, **Figure 4B**) and 3.31-fold more similar than the set of all SNPs (r = 0.131).
328 Meta-analyzed across the 21 traits, the marginal multi-ethnic effect size correlation among the
329 top 5% of IMPACT SNPs was significantly greater than the set of all SNPs genome-wide, across
330 the 10 most lenient of 17 GWAS locus P value thresholds examined (all difference of means $P <$
331 0.026) (**Figure 4C-D**). Furthermore, this observation was consistent across individual traits (**SF9**).
332 For comparison, we performed the same analysis using alternative annotations: lead
333 annotations from 513 cell-type-specifically expressed gene sets (SEG)[35] and 220 cell-type-
334 specific histone mark annotations (CTS)[6] (**SF10**). Marginal effect size correlation with IMPACT
335 was comparable to CTS when comparing the top 5% of SNPs to the set of all SNPs (difference of
336 means P value > 0.05 at 14 of 17 P value thresholds, **SF11**). Compared to SEG, IMPACT-selected
337 SNPs had a significantly greater correlation at 7 of 17 P value thresholds (all difference of means
338 P value < 0.02, **SF11**). Overall, our results suggest that we might anticipate improved trans-
339 ethnic portability of PRS models by prioritizing SNPs in key IMPACT annotations.
340
341 Finally, we addressed our hypothesis that IMPACT annotations improve the trans-ethnic
342 portability of PRS (**Figure 1D-III**). For each of the 21 previously analyzed traits, we built a PRS
343 using effect size estimates from EUR summary statistics and applied it to predict phenotypes of
344 EAS individuals from BioBank Japan (BBJ) (**Figure 5A**). Here, we compare two PRS models, both
345 blind to any EAS genetic or functional information and removing SNPs with LD r^2> 0.2,

Figure 4

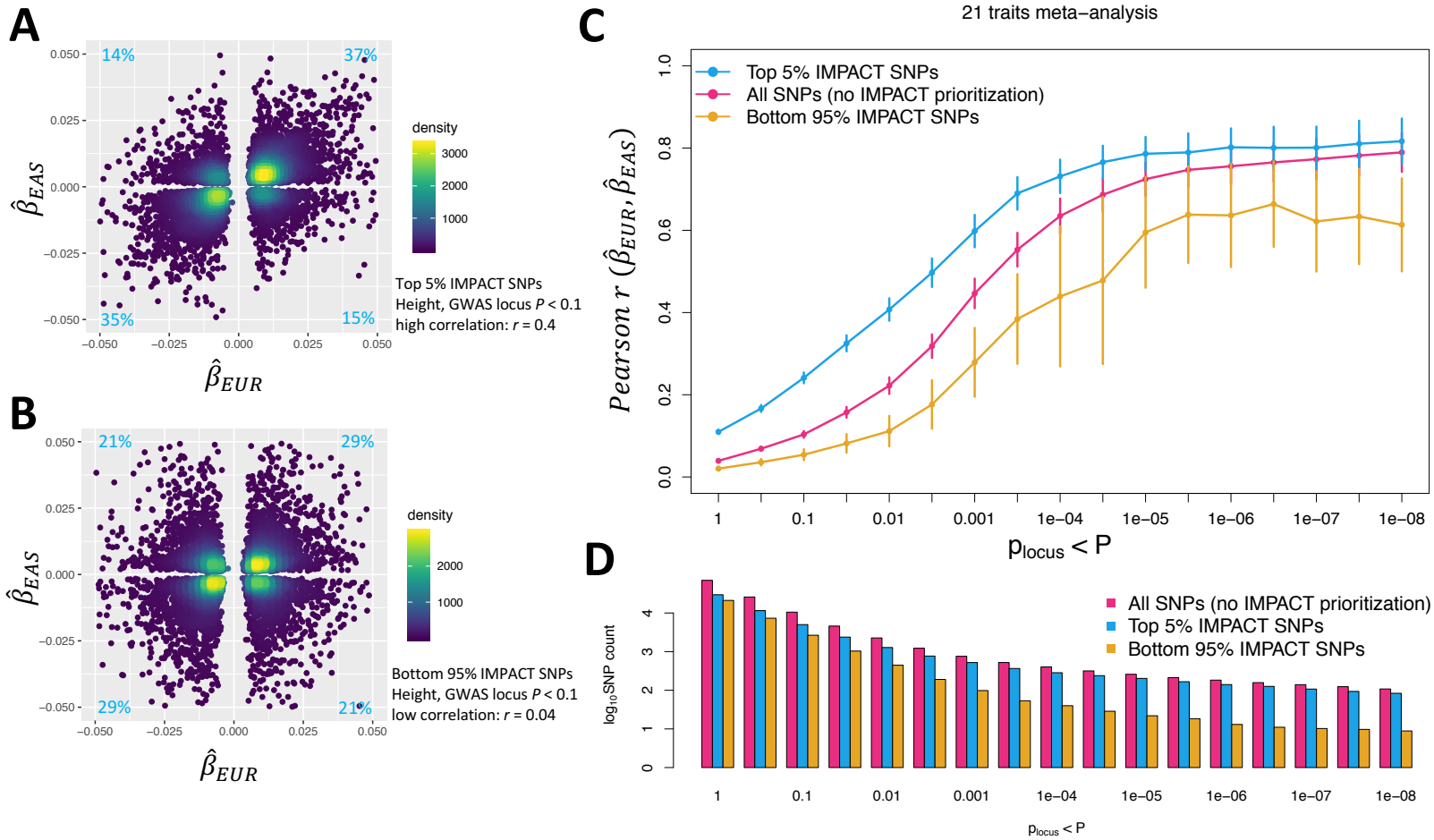

Figure 4 legend. Mechanism by which IMPACT prioritization of shared regulatory variants might improve trans-ethnic PRS performance. A) Estimated effect sizes of variants from genome-wide EUR and EAS height summary statistics in the top 5% of the lead IMPACT annotation for EUR height. Proportions of variants in each quadrant indicated in light blue. B) Estimated effect sizes from genome-wide EUR and EAS height summary statistics of variants in the bottom 95% of the same lead IMPACT annotation for height; mutually exclusive with SNPs in A). C) Meta-analysis of multi-ethnic marginal effect size correlations between populations across 21 traits shared between EUR and EAS cohorts over 17 GWAS *P* value thresholds (with reference to the EUR GWAS). D) Number of SNPs ($\log_{10}$ scale) at each *P* value threshold for each partition of the genome corresponding to C).

346 according to European individuals from phase 3 of 1000 Genomes[52]: (i) standard P+T PRS and
347 (ii) functionally-informed P+T PRS using a subset of SNPs prioritized by the lead EUR IMPACT
348 annotation (**Online Methods**). In functionally-informed PRS models, for each trait separately,
349 we *a priori* selected the subset of top-ranked IMPACT SNPs (top 1%, 5%, 10%, or 50%) which
350 explained the closest to 50% of total trait heritability (**Online Methods**). For all PRS models, we
351 report results from the most accurate model across nine EUR GWAS *P* value thresholds.

352 For each trait, we observed that functionally-informed PRS using IMPACT captured more
353 phenotypic variance than standard PRS (49.9% mean relative increase in R^2, **Figure 5B**, **SF12**,
354 **ST13-15**). The mean phenotypic variance explained across traits by functionally-informed PRS
355 (R^2 = 2.1%, se = 0.2%) was greater than by standard PRS (R^2 = 1.5%, se = 0.1%). For 20 of 21
356 traits, e.g. excluding basophil count, IMPACT-informed PRS significantly outperformed standard
357 PRS (difference of means $P < 0.01$). Using 10,000 bootstraps of the PRS sample cohort, we
358 found that the IMPACT-informed PRS R^2 estimate was consistently greater than the standard
359 PRS estimate for the same 20 traits (all bootstrap $P < 0.004$, **ST15**). We observed the largest
360 improvement for RA from R^2 = 1.4% (sd = 0.33%) in the standard PRS versus R^2 = 4.1% (sd =
361 0.53%, difference of means $P < 7.7e-10$) in the functionally-informed PRS using the B cell TBP
362 IMPACT annotation. For asthma, R^2 = 0.37% (sd = 0.10%) in the standard PRS versus R^2 = 0.75%
363 (sd = 0.14%, $P < 8.5e-4$) in the functionally-informed PRS. For MCV, R^2 = 3.0% (sd = 0.10%) in
364 the standard PRS versus R^2 = 4.1% (sd = 0.12%, $P < 1.9e-25$) in the functionally-informed PRS.
365 For PrCa, R^2 = 4.5% (sd = 0.36%) in the standard PRS versus R^2 = 6.4% (sd = 0.45%, $P < 2.4e-6$) in
366 the functionally-informed PRS. For height, R^2 = 4.2% (sd = 0.10%) in the standard PRS versus R^2
367 = 5.6% (sd = 0.12%, $P < 1.2e-37$) in the functionally-informed PRS.

368 For our five representative traits asthma, RA, MCV, PrCa, and height, we further
369 compared functionally-informed PRS_{EUR} using IMPACT to models using cell-type-specifically
370 expressed genes (SEG) and cell-type-specific histone modification tracks (CTS)[6,35] (**Figure 5C**,
371 **ST16**). Across all of the five traits, models using IMPACT explained significantly greater
372 phenotypic variance (mean R^2= 4.2%, se = 0.3%) than SEG (0.9%, se = 0.1%, all difference of
373 means *P* < 9.9e-11). While IMPACT generally outperformed CTS (R^2= 2.6%, se = 0.2%, difference
374 of means meta *P* < 1.2e-8), this observation was only individually consistent with 3 of 5 traits
375 (difference of means *P* < 9.3e-8). We performed a similar bootstrap analysis as above, yielding
376 similar results; for only RA and asthma did IMPACT-PRS not produce consistently greater
377 R^2estimates than CTS-PRS (**ST16**).
378 Functionally-informed PRS might to some extent compensate for population-specific LD
379 differences between populations. Hence, we hypothesized that IMPACT-informed PRS would
380 improve standard PRS moreso in the trans-ethnic prediction framework, in which EUR PRS
381 models predict EAS phenotypes, than in a within-population framework, in which EAS PRS
382 models predict EAS phenotypes. Here, we define within-population PRS as PRS_{EAS} and trans-
383 ethnic PRS as PRS_{EUR} to avoid confusion. In order to directly compare PRS model improvements
384 between PRS_{EAS} and PRS_{EUR}, we evaluated prediction accuracy on the same individuals. Briefly,
385 we partitioned the BBJ cohort to reserve 5,000 individuals for PRS testing, derived GWAS
386 summary statistics from the remaining individuals, and performed P+T PRS modeling and
387 prediction as done above (**Figure 5D, SF13-15, ST17-18, Online Methods**). For functionally-
388 informed PRS_{EAS}, we selected lead IMPACT annotations from S-LDSC results using GWAS
389 summary statistics, as done above, on the partition of the BBJ cohort excluding the 5,000 PRS
390 test individuals. We defined improvement as the percent increase in R^2 from standard to

391 functionally-informed PRS; therefore, differences in PRS performance due to intrinsic factors,
392 such as GWAS power or genotyping platform, cancel out. In both scenarios, we observed
393 significant non-zero improvements: averaged across the 21 traits in the trans-ethnic setting
394 (mean percent increase in R^2= 47.3%, se = 8.1%, *P* < 2.7e-9) and in the within-population
395 setting (mean percent increase in R^2= 20.9%, se = 6.6%, *P* < 7.5e-4). Indeed, this revealed a
396 significantly greater improvement in the trans-ethnic than in the within-population application
397 (difference of means *P* < 1.7e-4, **Figure 5E**).
398 Overall, our results reveal that functional prioritization of SNPs using IMPACT
399 significantly improves both trans-ethnic and within-population PRS models, but is especially
400 advantageous for the trans-ethnic application of PRS. In conclusion, our results nominate the
401 prioritization of SNPs according to functional annotations, especially using IMPACT, as a
402 potential tentative solution for the lack of trans-ethnic portability of PRS models. While
403 individuals of European ancestry dominate current genetic studies, population-nonspecific cell-
404 type-specific IMPACT annotations can help transfer highly powered EUR genetic data to study
405 still underserved populations.
406
407 **Discussion**
408
409 In this study, we created a compendium of 707 cell-type-specific regulatory annotations
410 (**Web Resources**) capturing disproportionately large amounts of polygenic heritability in 95
411 complex traits and diseases in EUR and EAS populations. We then proposed a three-step
412 framework to assess how well prioritization of regulatory variants with functional data can
413 improve multi-ethnic genetic comparisons. First, we showed that heritability-enriched

Figure 5

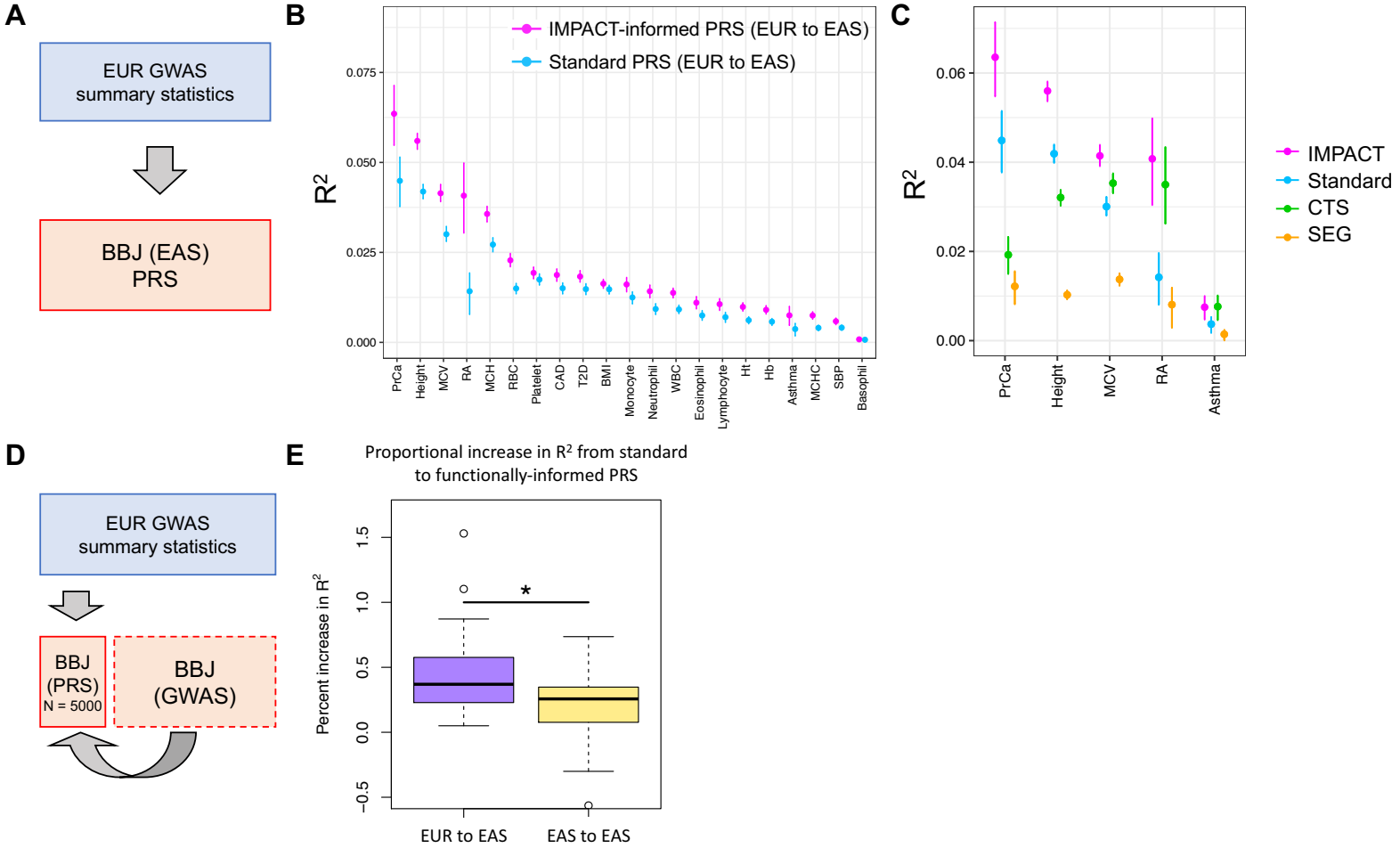

Figure 5 legend. Identifying shared regulatory variants with IMPACT annotations to improve the trans-ethnic portability of PRS. A) Study design applying EUR summary statistics-based PRS models to all individuals in the BBJ cohort. (B) Phenotypic variance (R^2) of BBJ individuals explained by EUR PRS using two methods: functionally-informed PRS with IMPACT (pink) and standard PRS (blue). Error bars indicate 95% CI calculated via 1,000 bootstraps. C) Phenotypic variance (R^2) of BBJ individuals across 5 exemplary traits explained by EUR IMPACT annotations relative to lead cell-type-specific histone modification annotations (CTS) and lead cell-type-specifically expressed gene sets (SEG). Error bars indicate 95% CI calculated via 1,000 bootstraps. D) Study design to compare trans-ethnic (EUR to EAS) to within-population (EAS to EAS) improvement afforded by functionally-informed PRS models. For each trait, 5,000 randomly selected individuals from BBJ designated as PRS samples. Remaining BBJ individuals used for GWAS to derive EAS summary statistics-based PRS; no shared individuals between GWAS samples and PRS samples. E) Improvement from standard PRS to functionally-informed PRS compared between trans-ethnic (EUR to EAS) and within-population models (EAS to EAS) using the study design in D).

414 regulatory elements between EUR and EAS populations capture indistinguishable proportions
415 of heritability across 29 complex traits. Second, we showed that functional prioritization of
416 variants selects those with more highly correlated marginal effect sizes between populations;
417 this might explain the improvement driven by functional prioritization in P+T PRS models which
418 use marginal effect sizes. Third, we showed that variant prioritization with IMPACT annotations
419 results in consistently improved PRS prediction accuracy, especially for the trans-ethnic
420 application; potentially due to overcoming large population-specific influences such as LD, an
421 important challenge of multi-population models.

422 Designing genetic models for each complex trait or disease that capture risk for the full
423 diversity of the human population will be challenging. This necessitates approaches that
424 effectively transfer predictive genetic information from well studied populations to less well
425 studied populations. Our work provides insight into the potential clinical implementation of PRS
426 and broader genetic applications that aim to integrate multi-ethnic data. We argue for the use
427 of biologically diverse IMPACT annotations to capture relevant genetic signal and compensate,
428 to some extent, for differences in LD across populations. While we did not assess a PRS model
429 using meta-analyzed summary statistics from two or more populations in this study, we believe
430 that this approach could be effective, especially for populations with limited GWAS sample size.

431 We believe that IMPACT may prioritize phenotype-driving regulatory variation. We have
432 shown IMPACT to be more effective at capturing genetic variation of complex traits than
433 commonly used functional annotations such as experimentally-derived cell-type-specific
434 histone marks or gene sets. We hypothesize the utility of IMPACT comes from 1) cell-type-
435 specificity of TF binding models which locate key classes of regulatory elements and 2) the
436 integration of thousands of experimentally-derived annotations, which presumably removes

437 noise and enriches for biological signal present in each individual annotation. Here, we did not
438 demonstrate the potential utility of IMPACT to perform functional fine-mapping to reduce
439 credible sets beyond our previous work[31], due to lack of sufficient gold standards with causal
440 experimental validation and the limitation to genome-wide significant variants. The specific
441 application of IMPACT in multi-ethnic fine-mapping needs to be further investigated.

442 We must consider several important limitations of our work. First, our functional
443 insights are limited to cell types with publicly available TF ChIP-seq data, lacking ones that are
444 rarer or more difficult to assay. In the future, the cell-type-specific functional training data for
445 IMPACT may be replaced by newer experimental strategies to map enhancers. For example,
446 high-throughput CRISPR screens paired with assays for open chromatin could be used to
447 precisely redefine the regulatory landscape. Second, we used multi-ethnic data to argue for the
448 utility of our approach. However, the robustness of multi-ethnic comparisons for a given
449 phenotype rely on properties surrounding the recruitment of individuals or the exact
450 genotyping platform used in various biobanks, which may result in cohort-bias that inflates
451 within-population PRS prediction accuracy. For example, BBJ is a disease ascertainment cohort,
452 in which each individual has any one of 47 common diseases[53,54]; therefore, BBJ control
453 samples are not comparable to healthy controls of UKBB. Other biases may arise from clinical
454 differences in phenotyping. Also, we only considered a single non-EUR population in this study,
455 while the disparity in trans-ethnic portability and hence resulting benefit from functional
456 annotations may be greater in other non-EUR populations.

457 In conclusion, we demonstrated that IMPACT annotations improve the comparison of
458 genetic data between populations and trans-ethnic portability of PRS models using ancestrally
459 unmatched data. While a long-term goal of the field must be to diversify GWAS and other

genetic studies in non-European populations, it is imperative that genetic models be developed that work in multiple populations. Such initiatives will necessitate the use of population-independent functional annotations, such as IMPACT, in order to capture shared biological mechanisms regulated by complex genetic variation.

Supplemental Data

See *Supplement.pdf* and *Supplementary_Tables.xlsx*

Online Methods

See *Online_Methods.pdf*

Acknowledgements

This work is supported in part by funding from the National Institutes of Health (NHGRI T32 HG002295, UH2AR067677, 1U01HG009088, U01 HG009379, and 1R01AR063759) and the Doris Duke Charitable Foundation grant #2013097.

Declaration of Interests

The authors declare no competing financial interests.

Web Resources

1. IMPACT 707 annotations: https://github.com/immunogenomics/IMPACT/tree/master/IMPACT707
2. IMPACT Github repository: https://github.com/immunogenomics/IMPACT

3. HOMER: http://homer.ucsd.edu/homer/motif/
4. S-LDSC: https://github.com/bulik/ldsc
5. 1000 Genomes: http://www.internationalgenome.org/
6. Cell-type-specifically expressed gene set annotations and LD scores: https://data.broadinstitute.org/alkesgroup/LDSCORE/LDSC_SEG_ldscores/
7. Cell-type-specific histone modification ChIP-seq datasets: https://data.broadinstitute.org/alkesgroup/LDSCORE/
8. Plink: https://www.cog-genomics.org/plink2

References

1. Kichaev, G. & Pasaniuc, B. Leveraging Functional-Annotation Data in Trans-ethnic Fine-Mapping Studies. *Am. J. Hum. Genet.* **97**, 260–271 (2015).
2. Lam, M. *et al.* Comparative genetic architectures of schizophrenia in East Asian and European populations. doi:10.1101/445874
3. Martin, A. R. *et al.* Clinical use of current polygenic risk scores may exacerbate health disparities. *Nat. Genet.* **51**, 584–591 (2019).
4. Sirugo, G., Williams, S. M. & Tishkoff, S. A. The Missing Diversity in Human Genetic Studies. *Cell* **177**, 26–31 (2019).
5. Vilhjálmsson, B. J. *et al.* Modeling Linkage Disequilibrium Increases Accuracy of Polygenic Risk Scores. *Am. J. Hum. Genet.* **97**, 576–592 (2015).
6. Finucane, H. K. *et al.* Partitioning heritability by functional annotation using genome-wide association summary statistics. *Nat. Genet.* **47**, 1228–1235 (2015).

507 7. Bulik-Sullivan, B. K. *et al.* LD Score regression distinguishes confounding from polygenicity
508 in genome-wide association studies. *Nat. Genet.* **47**, 291–295 (2015).
509 8. International Schizophrenia Consortium *et al.* Common polygenic variation contributes to
510 risk of schizophrenia and bipolar disorder. *Nature* **460**, 748–752 (2009).
511 9. Chatterjee, N., Shi, J. & García-Closas, M. Developing and evaluating polygenic risk
512 prediction models for stratified disease prevention. *Nat. Rev. Genet.* **17**, 392–406 (2016).
513 10. Stahl, E. A. *et al.* Bayesian inference analyses of the polygenic architecture of rheumatoid
514 arthritis. *Nat. Genet.* **44**, 483–489 (2012).
515 11. Chatterjee, N. *et al.* Projecting the performance of risk prediction based on polygenic
516 analyses of genome-wide association studies. *Nat. Genet.* **45**, 400–5, 405e1–3 (2013).
517 12. Khera, A. V. *et al.* Genome-wide polygenic scores for common diseases identify individuals
518 with risk equivalent to monogenic mutations. *Nat. Genet.* **50**, 1219–1224 (2018).
519 13. Schumacher, F. R. *et al.* Association analyses of more than 140,000 men identify 63 new
520 prostate cancer susceptibility loci. *Nat. Genet.* **50**, 928–936 (2018).
521 14. Sharp, S. A. *et al.* Development and Standardization of an Improved Type 1 Diabetes
522 Genetic Risk Score for Use in Newborn Screening and Incident Diagnosis. *Diabetes Care* **42**,
523 200–207 (2019).
524 15. Kullo, I. J. *et al.* Incorporating a Genetic Risk Score Into Coronary Heart Disease Risk
525 Estimates: Effect on Low-Density Lipoprotein Cholesterol Levels (the MI-GENES Clinical
526 Trial). *Circulation* **133**, 1181–1188 (2016).
527 16. Natarajan, P. *et al.* Polygenic Risk Score Identifies Subgroup With Higher Burden of
528 Atherosclerosis and Greater Relative Benefit From Statin Therapy in the Primary
529 Prevention Setting. *Circulation* **135**, 2091–2101 (2017).

530 17. Márquez-Luna, C., Loh, P.-R., South Asian Type 2 Diabetes (SAT2D) Consortium, SIGMA
531 Type 2 Diabetes Consortium & Price, A. L. Multiethnic polygenic risk scores improve risk
532 prediction in diverse populations. *Genet. Epidemiol.* **41**, 811–823 (2017).
533 18. Duncan, L. *et al.* Analysis of polygenic risk score usage and performance in diverse human
534 populations. *Nat. Commun.* **10**, 3328 (2019).
535 19. Hu, Y. *et al.* Leveraging functional annotations in genetic risk prediction for human
536 complex diseases. *PLoS Comput. Biol.* **13**, e1005589 (2017).
537 20. Márquez-Luna, C. *et al.* Modeling functional enrichment improves polygenic prediction
538 accuracy in UK Biobank and 23andMe data sets. *bioRxiv* 375337 (2018).
539 doi:10.1101/375337
540 21. Okada, Y. *et al.* Genetics of rheumatoid arthritis contributes to biology and drug discovery.
541 *Nature* **506**, 376–381 (2014).
542 22. Kanai, M. *et al.* Genetic analysis of quantitative traits in the Japanese population links cell
543 types to complex human diseases. *Nature Genetics* **50**, 390–400 (2018).
544 23. Yengo, L. *et al.* Meta-analysis of genome-wide association studies for height and body
545 mass index in ~700000 individuals of European ancestry. *Hum. Mol. Genet.* **27**, 3641–3649
546 (2018).
547 24. Schaub, M. A., Boyle, A. P., Kundaje, A., Batzoglou, S. & Snyder, M. Linking disease
548 associations with regulatory information in the human genome. *Genome Res.* **22**, 1748–
549 1759 (2012).
550 25. Maurano, M. T. *et al.* Systematic localization of common disease-associated variation in
551 regulatory DNA. *Science* **337**, 1190–1195 (2012).
552 26. Reshef, Y. A. *et al.* Detecting genome-wide directional effects of transcription factor

553 binding on polygenic disease risk. *Nat. Genet.* **50**, 1483–1493 (2018).

554 27. Liu, X., Li, Y. I. & Pritchard, J. K. Trans Effects on Gene Expression Can Drive Omnigenic
555 Inheritance. *Cell* **177**, 1022–1034.e6 (2019).

556 28. Lambert, S. A. *et al.* The Human Transcription Factors. *Cell* **172**, 650–665 (2018).

557 29. Teytelman, L., Thurtle, D. M., Rine, J. & van Oudenaarden, A. Highly expressed loci are
558 vulnerable to misleading ChIP localization of multiple unrelated proteins. *Proc. Natl. Acad.*
559 *Sci. U. S. A.* **110**, 18602–18607 (2013).

560 30. Skene, P. J. & Henikoff, S. An efficient targeted nuclease strategy for high-resolution
561 mapping of DNA binding sites. *Elife* **6**, (2017).

562 31. Amariuta, T. *et al.* IMPACT: Genomic Annotation of Cell-State-Specific Regulatory Elements
563 Inferred from the Epigenome of Bound Transcription Factors. *Am. J. Hum. Genet.* **104**,
564 879–895 (2019).

565 32. Kawakami, E., Nakaoka, S., Ohta, T. & Kitano, H. Weighted enrichment method for
566 prediction of transcription regulators from transcriptome and global chromatin
567 immunoprecipitation data. *Nucleic Acids Res.* **44**, 5010–5021 (2016).

568 33. ENCODE Project Consortium. An integrated encyclopedia of DNA elements in the human
569 genome. *Nature* **489**, 57–74 (2012).

570 34. Roadmap Epigenomics, C. *et al.* Heravi-428 Moussavi A, Kheradpour P, Zhang Z, Wang J, et
571 al. Integrative analysis of 111 reference human 429 epigenomes. *Nature* **518**, 317–330
572 (2015).

573 35. Finucane, H. K. *et al.* Heritability enrichment of specifically expressed genes identifies
574 disease-relevant tissues and cell types. *Nat. Genet.* **50**, 621–629 (2018).

575 36. Gazal, S. *et al.* Linkage disequilibrium–dependent architecture of human complex traits

576 shows action of negative selection. *Nat. Genet.* **49**, 1421–1427 (2017).

577 37. Buniello, A. *et al.* The NHGRI-EBI GWAS Catalog of published genome-wide association
578 studies, targeted arrays and summary statistics 2019. *Nucleic Acids Res.* **47**, D1005–D1012
579 (2019).

580 38. Akiyama, M. *et al.* Characterizing rare and low-frequency height-associated variants in the
581 Japanese population. *Nat. Commun.* **10**, 4393 (2019).

582 39. Ishigaki, K., Akiyama, M., Kanai, M. & Takahashi, A. Large scale genome-wide association
583 study in a Japanese population identified 45 novel susceptibility loci for 22 diseases.
584 *bioRxiv* (2019).

585 40. Akiyama, M. *et al.* Genome-wide association study identifies 112 new loci for body mass
586 index in the Japanese population. *Nat. Genet.* **49**, 1458–1467 (2017).

587 41. Brown, B. C., Ye, C. J., Price, A. L. & Zaitlen, N. Transethnic Genetic-Correlation Estimates
588 from Summary Statistics. *Am. J. Hum. Genet.* **99**, 76–88 (2016).

589 42. Drake, L. Y. *et al.* B cells play key roles in th2-type airway immune responses in mice
590 exposed to natural airborne allergens. *PLoS One* **10**, e0121660 (2015).

591 43. Amariuta, T., Luo, Y., Knevel, R., Okada, Y. & Raychaudhuri, S. Advances in genetics toward
592 identifying pathogenic cell states of rheumatoid arthritis. *Immunol. Rev.* (2019).
593 doi:10.1111/imr.12827

594 44. Buttari, B., Profumo, E. & Riganò, R. Crosstalk between red blood cells and the immune
595 system and its impact on atherosclerosis. *Biomed Res. Int.* **2015**, 616834 (2015).

596 45. Anderson, H. L., Brodsky, I. E. & Mangalmurti, N. S. The Evolving Erythrocyte: Red Blood
597 Cells as Modulators of Innate Immunity. *J. Immunol.* **201**, 1343–1351 (2018).

598 46. Lui, J. C. & Baron, J. Mechanisms limiting body growth in mammals. *Endocr. Rev.* **32**, 422–

599 440 (2011).

600 47. Maier, A. B., van Heemst, D. & Westendorp, R. G. J. Relation between body height and
601 replicative capacity of human fibroblasts in nonagenarians. *J. Gerontol. A Biol. Sci. Med.*
602 *Sci.* **63**, 43–45 (2008).

603 48. Murphy, R. A. *et al.* Adipose tissue, muscle, and function: potential mediators of
604 associations between body weight and mortality in older adults with type 2 diabetes.
605 *Diabetes Care* **37**, 3213–3219 (2014).

606 49. Heymsfield, S. B., Gallagher, D., Mayer, L., Beetsch, J. & Pietrobelli, A. Scaling of human
607 body composition to stature: new insights into body mass index. *Am. J. Clin. Nutr.* **86**, 82–
608 91 (2007).

609 50. Kichaev, G. *et al.* Leveraging Polygenic Functional Enrichment to Improve GWAS Power.
610 *Am. J. Hum. Genet.* **104**, 65–75 (2019).

611 51. Gusev, A. *et al.* Atlas of prostate cancer heritability in European and African-American men
612 pinpoints tissue-specific regulation. *Nat. Commun.* **7**, 10979 (2016).

613 52. Gibbs, R. A. *et al.* A global reference for human genetic variation. *Nature* **526**, 68–74
614 (2015).

615 53. Nagai, A. *et al.* Overview of the BioBank Japan Project: Study design and profile. *J.*
616 *Epidemiol.* **27**, S2–S8 (2017).

617 54. Hirata, M. *et al.* Cross-sectional analysis of BioBank Japan clinical data: A large cohort of
618 200,000 patients with 47 common diseases. *J. Epidemiol.* **27**, S9–S21 (2017).

Online Methods

Data

TF ChIP-seq data. We previously collected 3,181 publicly available transcription factor (TF) chromatin immunoprecipitation (ChIP) datasets derived from human primary cells or cell lines. We downloaded raw sequencing data in SRA format from NCBI GEO, then converted the data to FASTQ format using the SRA Toolkit function fastq-dump, used FastQC for quality assessment of sequencing reads, and finally mapped reads to the human genome (hg19/GRCh37) with Bowtie2 [v2.2.5] using default parameters. All ChIP-seq datasets were matched to corresponding control data from which peaks were called with macs [v2.1] with q value < 0.01 under a bimodal model, producing 3,181 bed file-formatted files[1,2]. The 1,542 datasets selected for use with our IMPACT model framework (see below) are listed with accession codes in **ST1**.

Genome-wide annotation data. We augmented our set of 515 publicly available epigenomic and sequence feature annotations from our previous study[3] with 116 personally curated datasets from NCBI, 2,593 ENCODE histone ChIP-seq datasets and 2,121 ENCODE open chromatin DNase-seq datasets[4], all publicly available at the accessions provided in **ST2**. All files were collected in 6-column standard bed file format. This augmentation brought the total number of features to 5,345.

Genome-wide association data. We collected publicly available summary statistics data for 111 genome-wide association studies (GWAS) across separate cohorts of East Asian and European

individuals[5–7]. East Asian GWAS data were collected from Biobank Japan (BBJ) while European GWAS data were collected from either UKBioBank (UKBB) or the GWAS catalog, referred to as PASS (publicly available summary statistics) (**ST3**). All GWAS summary statistics were reformatted to be compatible with S-LDSC (see below) and thus contained the following information for each SNP (per row): rsID, A1 (reference allele), A2 (alternative allele), GWAS sample size (effective sample size per SNP, may vary with genotyping), chi-square statistic, *z*-score. For multi-ethnic genetic correlation and polygenic risk score prediction, all GWAS summary statistics were reformatted to contain the SNP ID (chr_position_A1_A2), chromosome, base pair, A1, A2, effect size estimate, effect size estimate standard error, and *P*-value.

Cell-type-specifically expressed gene set (SEG) and cell-type-specific histone modification (CTS) annotations. We downloaded 513 publicly available SEG annotations for European SNPs from phase 3 of 1000 Genomes accompanied by pre-computed LD scores (see **Web Resources**)[8]. SEG annotations are binary and thus each SNP is designated a 1 or a 0, indicating that the SNP does or does not lie, respectively, within 100 kb of the gene body of the corresponding gene set[8]. We downloaded 220 publicly available CTS annotations of peak data in bed file format, from which we annotated European SNPs from phase 3 of 1000 Genomes[9] and used S-LDSC to compute LD scores (see **Web Resources**)[7]. These annotations are also binary, in which case each SNP is designated a 1 or a 0, indicating that the SNP does or does not like, respectively, within the peak of histone modification.

45 ***BioBank Japan data.*** For PRS analysis, we utilized phenotype and genotype data of the BioBank
46 Japan Project (BBJ)[10,11]. All of the calculations related to PRS were conducted on the RIKEN
47 computing server. BBJ is a biobank that collaboratively collects DNA and serum samples from
48 12 medical institutions in Japan. This project recruited approximately 200,000 patients with the
49 diagnosis of at least one of 47 diseases. Informed consent was obtained from all participants by
50 following the protocols approved by their institutional ethical committees. We obtained
51 approval from the ethics committees of the RIKEN Center for Integrative Medical Sciences and
52 the Institute of Medical Sciences at the University of Tokyo.
53
54 **Statistical Methods**
55
56 ***IMPACT Model.*** We implemented our previously defined model to predict TF binding on a motif
57 site. This model regresses the likelihood (*p*) of a binding event on the epigenomic profile of the
58 motif site, in a logistic regression framework over *j* epigenomic features as follows:
59 $$log\ (\frac{p}{1-p})\ =\ \beta_0 + \beta_1 X_1 + \beta_2 X_2 + \ldots + \beta_j X_j.$$
60 We use a weighted average of ridge and lasso regularization terms in the objective function to
61 restrict the magnitude of fit coefficients and enforce sparsity to reduce overfitting, respectively,
62 as follows:
63
64 $$argmin_\beta\ =\ (||Y\ -\ X\beta||^2\ +\ \frac{1}{2}(1\ -\ \alpha)||\beta||^2\ +\alpha\ ||\beta||).$$
65

66 ***Training IMPACT.*** We trained an IMPACT model for each unique cell type-TF pair present in our
67 data collection. Our collection consists of 3,181 TF ChIP-seq profiles, representing 442 TFs, 296
68 cell types, and 24 tissues. The IMPACT model requires that the assayed TF has a distinct binding
69 motif and so we removed all ChIP-seq datasets corresponding to a TF that did not have a known
70 sequence motif in MEME, Jaspar, or Transfac databases. This resulted in 1,542 TF ChIP-seq
71 profiles across 142 TFs, 245 cell types, 23 tissues, and 728 unique combinations of TFs and cell
72 types. As we did in our previous study[3], we merged experiments of the same TF-cell type
73 combination by taking the union of the peaks. We next identified motif sites bound by a TF by
74 using HOMER [v4.8.3][12] to scan ChIP-seq peaks for motif matches exceeding the empirically
75 determined motif detection threshold. Similarly, we identified motif sites not bound by a TF by
76 using HOMER to scan the entire genome for sequence matches. 21 of these models did not
77 contain sufficient overlap between TF sequence motifs and ChIP-seq peaks which would lead to
78 underfitting in the logistic regression (fewer than 7), thereby resulting in 707 total possible
79 IMPACT annotations. We then trained 707 IMPACT models using up to 1,000 TF-bound
80 sequence motifs (evidenced by ChIP-seq) and 10,000 unbound sequence motifs. For each of
81 707 TF-cell type pairs, we learned a predictive model of TF binding and annotated SNPs
82 genome-wide for both EUR and EAS populations, with a mean regulatory probability per
83 nucleotide of 0.02 (se = 7.5e-4).
84
85 ***Assessing cell type specificity of IMPACT tracks.*** We acquired lists of specifically expressed
86 genes in 9 different cell types: T cells, B cells, fibroblasts, monocytes, brain, liver, colon,
87 prostate, and breast according to differential gene expression *t*-statistics from previous work[8],

88 specifically labeled as T.4+8int.Th, B.Fo.LN, Cells_Transformed_fibroblasts, Mo.6C+II-.LN,
89 Brain_Cortex, Liver, Colon_Transverse, Prostate, Breast_Mammary_Tissue, respectively from
90 either ImmGen or GTEx databases. Large and positive *t*-statistics represent greater specificity of
91 gene expression in the target cell type, large but negative *t*-statistics represent specifically
92 repressed genes, and *t*-statistics near 0 represent nonspecific gene expression, representing
93 commonly expressed genes. For each cell type, we selected the 100 genes with highest *t*-
94 statistics, e.g. specifically expressed (SE) genes, and 100 genes such that $-0.5 < t\text{-statistic} < 0.5$,
95 e.g. not specifically expressed genes (NS). For each cell type separately, we collected all related
96 IMPACT annotations from the compendium of 707 total annotations. Then for each annotation
97 separately, we computed the average IMPACT score over all EUR SNPs from phase 3 of 1000
98 Genomes within 2kb of each SE or NS gene body. Finally, we computed the average across all
99 100 SE and 100 NS genes, separately.
100
101 ***Partitioning heritability with S-LDSC.*** We applied S-LDSC [v1.0.0][7] to partition the common
102 (MAF > 5%) SNP heritability of 111 polygenic traits and diseases, with significantly non-zero
103 heritability estimates ($P < 0.05$). We partitioned heritability using a customized version of the
104 baselineLD model, in which we excluded cell-type-specific regulatory annotations (as we would
105 be testing the enrichment of such annotations from IMPACT). In total, we used 69 cell-type-
106 nonspecific baselineLD annotations and added one or more IMPACT annotations to the model
107 to test for cell-type-specific enrichment. We use three metrics to evaluate how well our
108 IMPACT annotations capture polygenic heritability: enrichment[7], the proportion of heritability
109 explained by the top 5% of SNPs[7], and per-annotation standardized effect size, τ^*[6]. Briefly,

110 enrichment is defined as the proportion of common SNP heritability divided by the genome-
111 wide proportion of SNPs in the annotation, for continuous annotations this is the average
112 annotation value across SNPs. τ^* represents the average per-SNP heritability of a category of
113 SNPs, where a single SNP may claim membership to one or more categories. τ^* is defined as the
114 proportionate change in per-SNP heritability associated with a one standard deviation increase
115 in the value of the annotation. The sum of the τ^* over categories of SNPs equals the total
116 estimated heritability of the trait. τ^* has units of heritability and is comparable between traits,
117 annotations, and populations, because it is normalized for the total heritability (indicative of
118 the power of the GWAS), the dispersion of the annotation values (annotation size), and the
119 number of common SNPs (population-specific) considered in the model, respectively. τ, the
120 precursor of τ^*, is the coefficient estimated in the S-LDSC regression. τ and τ^* are conditionally
121 dependent on the provided baselineLD annotations. Therefore, the τ^* estimate for an IMPACT
122 annotation is considered a measure of cell-type-specific or annotation-specific SNP heritability,
123 as the remaining annotations in the model (baselineLD) are not cell-type-specific. Significance
124 of τ^* is computed using a *z*-test of how different the τ^* estimate is from 0; the significance of
125 strictly positive τ^* estimates are reported in our study.
126
127 ***Measuring heritability in top X% of SNPs of a continuous annotation.*** To partition the
128 heritability captured by various top echelons of SNPs of a given continuous annotation, we used
129 the same strategy as in a previous study[6]. By this strategy, the proportion of heritability
130 explained by a set of SNPs is the sum over all SNPs of the product of the τ^* of each category in
131 the S-LDSC model, e.g. baselineLD plus IMPACT annotation, and the SNP membership to that

132 category (1 or 0 in the case of binary annotations, continuous values in the case of continuous
133 annotations) divided by the same metric for all SNPs genome-wide.
134
135 ***Conditional S-LDSC analysis to identify independent annotation-trait associations.*** Due to the
136 redundancy in modeled cell type programs and inherent covariance of IMPACT annotations
137 (**SF2**), the τ^* associations we find with S-LDSC cannot be independent. To this end, for each of
138 95 traits across EUR and EAS for which we identified a lead IMPACT annotation, reported in
139 **ST9**, we performed a series of conditional analyses using S-LDSC. For each trait with more than
140 one significant τ^* association, we created S-LDSC models consisting of the 69 baselineLD
141 annotations, the lead annotation for that trait, and separately, each remaining significant
142 IMPACT annotation. We kept annotations that retained their τ^* significance when conditioned
143 on the lead annotation(s), which we also required to retain significance. We iteratively
144 performed these conditional analyses until we were no longer able to identify independent τ^*
145 associations.
146
147 ***Deming regression of EUR τ^* on EAS τ^*.*** As there is significant correlation among IMPACT
148 annotations, due to redundancy in cell type regulatory elements, we used an iterative pruning
149 approach, similar to LD-pruning, to identify independent IMPACT annotations. For each trait,
150 we ranked all 707 IMPACT annotations by their τ^* significance values. Then, we selected the
151 lead annotation, removed all annotations correlated with Pearson $r > 0.5$, and selected the next
152 lead annotation, and so on. This approach produced a set of relatively independent
153 annotations, for which the assumptions of Deming, or any, regression would not be violated.

154 For each trait, we ran Deming regression over approximately 100 independent IMPACT
155 annotations using the R function *deming* within the package *deming*. Across independent
156 observations for all traits, we tested the null hypothesis that the slope of the Deming
157 regression, which considers standard errors on both the predictor (EUR τ*) and response
158 variables (EAS τ*), is equal to 1.
159
160 ***Multi-ethnic and within-population genetic correlation.*** We computed the genetic correlation
161 (R_g) between pairs of 29 traits for which we acquired EUR and EAS GWAS using Popcorn
162 [v.0.9.6][13] with default parameters, including maximum likelihood estimation as opposed to
163 regression[14]. First, we computed cross-population scores between the two populations using
164 the *compute* flag with the *popcorn* executable, indicating approximately the correlation
165 between LD at each SNP using EUR and EAS reference LD panels from phase 3 of 1000
166 Genomes. Then, we used the *fit* flag with the *popcorn* executable to compute the multi-ethnic
167 genetic correlation of these 29 traits. R_g estimates computed after restricting to MAF > 5% did
168 not significantly differ from no MAF restriction. Popcorn computes R_g using either "genetic
169 impact" (effect sizes normalized by allele frequency) or "genetic effect" (unmodified effect
170 sizes). We observed no significant heterogeneity between the R_g computed using "genetic
171 impact" and "effect", although "genetic effect" estimates were consistently but not significantly
172 larger.
173 We then computed cross-trait cross-population genetic correlations across 21 traits for
174 which we observed at least one significant IMPACT annotation association in both EUR and EAS.
175 Therefore, in total we computed the genetic correlation among 42 traits (21 phenotypes x 2

176 populations). For pairs of traits with one from EUR and one from EAS, we used Popcorn as
177 described above with MAF threshold of 5% and "genetic impact". For pairs of traits from the
178 same population we used LDSC [v.1.0.0]. First we used the *munge_sumstats.py* script to make
179 the direction of allelic effect consistent in the GWAS summary statistics while also restricting to
180 well-imputed Hapmap3 SNPs. Then, we used the *ldsc.py* script with the *-rg* flag to compute the
181 genetic correlation using EUR and EAS reference LD panels from phase 3 of 1000 Genomes
182 where appropriate.
183
184 ***Multi-ethnic marginal effect size correlation.*** We acquired GWAS summary statistics for each
185 of 21 shared traits between EUR and EAS for which there was at least one significant IMPACT
186 association in each population. Then, we restricted to SNPs shared between EUR and EAS
187 GWAS summary statistics. Next, we performed stringent iterative LD clumping with PLINK
188 [v1.90b3][15] using EUR summary statistics (selecting the most significant SNP, then removing all
189 SNPs in LD with r^2 > 0.1 within 1 Mb, then selecting the next most significant SNP, and so on).
190 This step satisfies the assumption of independence in the Pearson correlation that we will
191 compute among marginal effect sizes. We selected our initial set of SNPs under three scenarios:
192 (1) using no functional inference, (2) using the top 5% of SNPs according to the trait's lead EUR
193 IMPACT annotation, and (3) using the bottom 95% of SNPs according to the trait's lead EUR
194 IMPACT annotation (mutually exclusive with scenario 2). With our set of independent SNPs for
195 each trait and under each of three scenarios, we compute a Pearson correlation between the
196 estimated effect sizes, while further stratifying loci on 17 EUR *P*-values (1, 0.3, 0.1, 0.03, 0.01,

197 3e-3, 1e-3, 3e-4, 1e-4, 3e-5, 1e-5, 3e-6, 1e-6, 3e-7, 1e-7, 3e-8, 1e-8). For example, stratum with

198 P = 0.1 includes all SNPs with EUR GWAS P < 0.1.

199

200 ***Polygenic risk score calculation.*** In this study, we utilized pruning and thresholding (P+T) for the

201 calculation of PRS. We constructed PRS models from either EUR summary statistics or EAS

202 summary statistics and evaluated their predictive performance on individual EAS phenotypes.

203 Here, we define within-population PRS as PRS_{EAS} and trans-ethnic PRS as PRS_{EUR} to avoid

204 confusion. For PRS_{EUR}, we utilized genome-wide summary statistics from EUR as reported in

205 their publicly available version. For PRS_{EAS}, we held out 5,000 individuals for PRS analysis and

206 conducted GWAS using the remaining individuals to avoid overfitting (see next section). For

207 each trait separately, we restricted our analysis to variants that exist in both GWAS summary

208 statistics and post-imputation genotype data of EAS individuals used for PRS analysis

209 (imputation quality of r^2 > 0.3 in minimac3). A detailed description related to the genotyping

210 platform and imputation strategy is provided in a previous report[2]. We excluded the MHC

211 region in this analysis.

212 We designed PRS models using two strategies: standard PRS and functionally-informed

213 PRS. For standard PRS_{EUR}, we performed conventional LD clumping to acquire sets of

214 independent SNPs using EUR LD reference panels from phase3 of 1000 Genomes. Similarly for

215 PRS_{EAS}, we utilized EAS LD reference panels from phase3 of 1000 Genomes. We used PLINK

216 [v1.90b3][15] to remove variants in LD with r^2 > 0.2 with a significance threshold for index SNPs

217 of P = 0.5. For functionally-informed PRS, we restricted the analysis to variants with high

218 IMPACT score according to the lead IMPACT annotation before conducting LD clumping. As

219 before, we define the lead annotation as the one with the largest τ^* estimate that was
220 significantly greater than 0. When we designed PRS_{EUR}, we utilized the lead IMPACT annotation
221 in EUR GWAS summary statistics (EAS summary statistics were not taken into account to avoid
222 overfitting). Similarly, when we design PRS_{EAS}, we utilized the lead IMPACT annotation in EAS
223 GWAS summary statistics for which 5,000 EAS individuals for PRS analysis were removed to
224 avoid overfitting. We performed LD clumping using variants within a predefined top percentage
225 of IMPACT scores. This was determined by the percentage that captured the closest to 50% of
226 total trait heritability; considered percentages included the top 1%, 5%, 10%, and 50%.

227 We evaluated PRS performance using EAS individuals. First, we used all individuals in the
228 BBJ cohort for PRS_{EUR} testing. Second, we compared the improvement afforded by IMPACT in
229 PRS_{EUR} relative to PRS_{EAS} models using 5,000 randomly selected individuals in BBJ; specifically
230 for case-control GWAS, we randomly selected 1,000 cases and 4,000 controls.

231 For all models, we built a PRS for each individual *j* in our test set (in all cases, there is no
232 overlap between GWAS samples and PRS samples) using variant effect size estimates from
233 GWAS as follows:

234 $$PRS_j = \sum_i^M A_i * \beta_i, \qquad \text{(Equation 1)}$$

235

236 Where M is the total number of SNPs shared between GWAS summary statistics and post-
237 imputation genotype data of EAS individuals, *i* is the ith SNP in the model, A_i is the allele dosage
238 of the trait-increasing allele *i*, and β_i is the estimated effect size of allele *i* from the GWAS. We
239 calculated PRS using PLINK2.

240 For QC of quantitative phenotypes, we excluded (1) related samples (PI_HAT > 0.187
241 estimated by PLINK), (2) samples with age < 18 and age > 85, and (3) samples with measured
242 values outside three interquartile ranges (IQR) of the upper or lower quartiles. The effect of sex,
243 age, age^2, the top 10 PCs, and affection status of 47 diseases were removed by linear
244 regression, and the residuals were further normalized by the rank-based inverse normal
245 transformation (see Equation 3 below). For QC of case/control phenotypes, we excluded (1)
246 related samples (PI_HAT > 0.187 estimated by PLINK) and (2) samples with age < 18 and age >
247 85.
248 We then regressed our phenotype of interest (Y), a measured quantitative trait or a
249 diagnosed disease among the PRS samples, on the per-individual PRS as follows:
250
251 For diseases,
252 $Y_j \sim PRS_j + sex + age + Geno\ PC1 + \ldots + Geno\ PC10.$ (Equation 2)
253 For quantitative traits,
254 $Normalized\ Y_j \sim PRS_j.$ (Equation 3)
255
256 We then report the variance explained; for quantitative traits, this is the variance
257 explained by a linear model and for diseases, the variance explained is from a logistic model
258 (Nagelkerke R^2)[14,16,17] which we convert to liability scale pseudo R^2 such that R^2 values are
259 comparable among both quantitative and case/control phenotypes. We used various GWAS *P*
260 value thresholds (0.1, 0.03, 0.01, 0.003, 0.001, 3e-4, 1e-4, 3e-5, 1e-5) to assess the predictive

261 performance of our PRS. For each model, we reported in the text the largest R^2achieved across
262 the nine P value thresholds.
263 To estimate confidence intervals of PRS performance (R^2, as explained above), we
264 conducted 1,000 bootstraps using the R package *boot*. We also conducted 10,000 bootstraps to
265 evaluate whether the R^2difference between two PRS models (functionally-informed - standard)
266 is significantly greater than 0; we calculated the R^2difference between two PRS models in each
267 round of bootstrapping (delta R^2), and assess its distribution in 10,000 bootstraps. If we let N
268 be the frequency of delta R^2< 0, we define one-sided *P* values for delta R^2> 0 as (N +
269 1)/10,000.
270
271 ***Genome-wide association studies in BBJ.*** As described in the previous section, we held out
272 5,000 randomly selected individuals for the PRS analysis and performed GWAS on the
273 remaining individuals (sample sizes are provided in **ST13-14**). GWAS was conducted with PLINK2
274 using the same imputed dosages as used in the PRS analysis. For quantitative traits, normalized
275 residuals were analyzed by a linear regression model. For diseases, affection status was
276 analyzed by a logistic regression model using age, sex, and the top 10 genotype PCs as
277 covariates.
278
279 **Online Methods References**

280 1. Kawakami, E., Nakaoka, S., Ohta, T. & Kitano, H. Weighted enrichment method for
281 prediction of transcription regulators from transcriptome and global chromatin
282 immunoprecipitation data. *Nucleic Acids Res.* **44**, 5010–5021 (2016).

283 2. Ishigaki, K., Akiyama, M., Kanai, M. & Takahashi, A. Large scale genome-wide association
284 study in a Japanese population identified 45 novel susceptibility loci for 22 diseases.
285 *bioRxiv* (2019).
286 3. Amariuta, T. *et al.* IMPACT: Genomic Annotation of Cell-State-Specific Regulatory Elements
287 Inferred from the Epigenome of Bound Transcription Factors. *Am. J. Hum. Genet.* **104**,
288 879–895 (2019).
289 4. ENCODE Project Consortium. An integrated encyclopedia of DNA elements in the human
290 genome. *Nature* **489**, 57–74 (2012).
291 5. Kanai, M. *et al.* Genetic analysis of quantitative traits in the Japanese population links cell
292 types to complex human diseases. *Nat. Genet.* **50**, 390–400 (2018).
293 6. Gazal, S. *et al.* Linkage disequilibrium–dependent architecture of human complex traits
294 shows action of negative selection. *Nat. Genet.* **49**, 1421–1427 (2017).
295 7. Finucane, H. K. *et al.* Partitioning heritability by functional annotation using genome-wide
296 association summary statistics. *Nat. Genet.* **47**, 1228–1235 (2015).
297 8. Finucane, H. K. *et al.* Heritability enrichment of specifically expressed genes identifies
298 disease-relevant tissues and cell types. *Nat. Genet.* **50**, 621–629 (2018).
299 9. Gibbs, R. A. *et al.* A global reference for human genetic variation. *Nature* **526**, 68–74
300 (2015).
301 10. Nagai, A. *et al.* Overview of the BioBank Japan Project: Study design and profile. *J.*
302 *Epidemiol.* **27**, S2–S8 (2017).
303 11. Hirata, M. *et al.* Cross-sectional analysis of BioBank Japan clinical data: A large cohort of
304 200,000 patients with 47 common diseases. *J. Epidemiol.* **27**, S9–S21 (2017).

305 12. Heinz, S. *et al.* Simple combinations of lineage-determining transcription factors prime cis-
306 regulatory elements required for macrophage and B cell identities. *Mol. Cell* **38**, 576–589
307 (2010).
308 13. Brown, B. C., Ye, C. J., Price, A. L., Zaitlen, N. & Asian Genetic Epidemiology Network-Type 2
309 Diabetes. Transethnic genetic correlation estimates from summary statistics.
310 doi:10.1101/036657
311 14. Martin, A. R. *et al.* Clinical use of current polygenic risk scores may exacerbate health
312 disparities. *Nat. Genet.* **51**, 584–591 (2019).
313 15. Purcell, S. *et al.* PLINK: a tool set for whole-genome association and population-based
314 linkage analyses. *Am. J. Hum. Genet.* **81**, 559–575 (2007).
315 16. Lam, M. *et al.* Comparative genetic architectures of schizophrenia in East Asian and
316 European populations. doi:10.1101/445874
317 17. Lee, S. H., Goddard, M. E., Wray, N. R. & Visscher, P. M. A better coefficient of
318 determination for genetic profile analysis. *Genet. Epidemiol.* **36**, 214–224 (2012).